Fundamental design principles for transcription-factor-based metabolite biosensors

Ahmad A. Mannan[1,+], Di Liu[2,+], Fuzhong Zhang[2,#] and Diego A. Oyarzún[1,#]

[1] Department of Mathematics, Imperial College London, UK
[2] Department of Energy, Environmental & Chemical Engineering, Washington University in St Louis, USA
[+] Equal contribution
[#] Corresponding authors: fzhang@seas.wustl.edu, d.oyarzun@imperial.ac.uk

Abstract. Metabolite biosensors are central to current efforts towards precision engineering of metabolism. Although most research has focused on building new biosensors, their tunability remains poorly understood and is a fundamental aspect for their broad applicability. Here we asked how genetic modifications shape the dose-response curve of biosensors based on metabolite-responsive transcription factors. Using the lac system in *Escherichia coli* as a model system, we built promoter libraries with variable operator sites that reveal interdependencies between biosensor dynamic range and response threshold. We developed a phenomenological theory to quantify such design constraints in biosensors with various architectures and tunable parameters. Our theory reveals a maximal achievable dynamic range and exposes tunable parameters for orthogonal control of dynamic range and response threshold. Our work sheds light on fundamental limits of synthetic biology designs and provides quantitative guidelines for biosensor design in applications such as dynamic pathway control, strain optimization, and real-time monitoring of metabolism.

Keywords: metabolite biosensor, dynamic pathway regulation, metabolic engineering, transcriptional regulator, pathway optimization, model-based design.

Introduction

A core principle in synthetic biology is the assembly of biological components into larger systems with predetermined functions. Metabolite biosensors, in particular, have received substantial attention because of their role in many applications at the interface of synthetic biology and metabolic engineering. Biosensors control gene expression in response to small molecules and provide a powerful tool to probe and control the metabolic state of a host. This makes them versatile for diverse applications, such as dynamic pathway engineering (1–4), high-throughput screening (5, 6) and complex genetic-metabolic circuitry (7).

A number of molecular mechanisms have been used for sensing intracellular metabolites, including e.g. RNA aptamers (8, 9) and metabolite-responsive transcription factors (TFs) (10, 11). The latter have become particularly popular because many organisms have evolved TFs that respond to native metabolites. In *E. coli*, for instance, about a third of TFs are known to respond to metabolites (12). Metabolite-responsive TFs can be re-purposed as biosensors in a different host (13) or re-engineered to respond to new ligands (14). The list of compounds for which biosensors have been developed is growing quickly (11) and includes precursors to biosynthetic pathways as well as products from secondary metabolism (15–19).

As illustrated in Figure 1A, for the purposes of biosensor design, metabolite-responsive TFs can be conceptualized as the composition of two modules: a sensing module for the interaction between the metabolite and the TF, and a regulation module where the TF controls the expression of a target gene. Biosensors generally have one of four different architectures, depending on the type of interactions of the sensing and regulation module. Examples of these biosensor architectures can be found across diverse applications in metabolic engineering, see e.g. the reviews in (10, 11) or Table SF2 in the Supplementary File S1.

Most applications require biosensors to be tunable, so that designers can adjust biosensor output to the expected physiological concentration of a metabolite. Common strategies for biosensor tuning target the sensing and regulation modules separately, either via protein engineering to modify the

binding kinetics between the metabolite and TF (14, 19), or promoter engineering to modify the transcriptional activity of the TF (20). Yet a major challenge for biosensor tuning is that their overall response compounds the effect of sensing and regulation, and thus changes to one component typically affect all parameters of the dose-response curve simultaneously (Figure 1B). As a result, biosensor design requires lengthy trial-and-error iterations between genetic modifications and strain characterization.

Previous studies have focused on the impact of transcriptional processes on the regulatory function of TFs (21, 22). Such studies have successfully used biophysical models to identify relations between parameters and the TF dose-response curve (23, 24). In the case of metabolite biosensors, however, their two-module architecture conflates the effect of metabolite sensing with the regulatory action of the TF. This makes it difficult to tease apart the impact of tunable parameters on the overall dose-response curve. This is especially relevant in metabolic engineering applications, where biosensors are typically built with sensing and regulation modules taken from different sources, both of which can be tuned independently and have diverse molecular mechanisms (10, 11). As a result, biosensor design can benefit from system-level descriptions that abstract from mechanistic details and highlight the input-output dependencies among components.

Here we sought to characterize the interdependency between tunable parameters and the dose-response curves of metabolite biosensors. Combining phenomenological modeling and strain characterization, we provide a simple theory for the design of metabolite biosensors with various architectures and tunable parameters. Our results highlight fundamental constraints in biosensor design and expose tunable parameters that facilitate precise control of biosensor function.

Results and Discussion

Design constraints in dose-response curves of metabolite biosensors

To study the relation between promoter tuning and biosensor function, we focused on metabolite-responsive TFs, the most widespread mechanism employed for sensing small molecules (10, 11, 25). In these biosensors, a convenient tunable parameter is the affinity of the TF to the promoter operator site, as it can be modified with rapid and cost-effective techniques such as random mutagenesis of promoter sequence or changes in operator copy number or location (25, 26).

As a model system for our investigation, we focused on the lactose inducible system in *Escherichia coli*. We built eight *lacUV5*-based promoters with different mutations at the LacI-binding operator site (sequences in Figure 1C). We incorporated a red fluorescent protein (*rfp*) gene downstream of each promoter and measured the dose-response curve to varying concentrations of Isopropyl β-D-1-thiogalactopyranoside (IPTG), a non-metabolizable compound that mimics allolactose and induces the lac promoter by allosteric binding to the LacI repressor. We characterized the dose-response curves of each strain though steady state RFP fluorescence in mid-exponential growth. The resulting dose-response curves display significant differences (Figure 1C), with basal fluorescence outputs spanning two orders of magnitude and up to two-fold changes in maximal biosensor output.

To quantify the differences among the biosensors, we computed their dose-response parameters as defined in Figure 1B. We found a strong interdependency between the biosensor parameters for varying operator sites. In particular, when dynamic range (μ) and threshold (θ) are plotted against each other (Figure 1D), we found a fundamental constraint for biosensor design. The constraint indicates that upon changes in operator affinity, biosensors with a broader dynamic range also display a larger response threshold. This suggests that tuning the promoter operator site can increase the dynamic range of the biosensor, but at the cost of simultaneously increasing the level of metabolite required to elicit a response.

To explain the observed constraint between threshold and dynamic range, we formulated a general mathematical model of the biosensors. Motivated by the modular description in Figure 1A, we used phenomenological models that describe the steady state of the sensing and regulation modules as Hill functions of their inputs. In the case of the lac system, which corresponds to the repressed-repressor architecture in Figure 1A, the model reads

$$f_1(M) = b_1 + \frac{a_1}{1 + (K_1 M)^{n_1}}, \qquad f_2(TF) = b_2 + \frac{a_2}{1 + (K_2 TF)^{n_2}}, \tag{1}$$

where f_1 is the concentration of functional TF that can bind to the operator site as a function of the metabolite concentration (M), and f_2 is the expression level of the target gene (P) as a function of the concentration of repressor. The parameters a_i, b_i, K_i, and n_i define the shape of the Hill curves for each module. In particular, the parameters b_1 and b_2 model the basal level of TF activity and promoter expression, respectively; parameters a_1 and a_2 are the maximum increase in TF activity and promoter expression, relative to their basal levels, respectively; parameter K_1 is the metabolite-TF affinity, and K_2 is the TF-operator affinity; and parameters n_1 and n_2 represent the sensitivity of metabolite-TF and TF-operator binding, respectively. Although specific molecular mechanisms can be well approximated by Hill functions similar to Eq. (1) (27–29), in this work we do not instance the models to specific mechanisms but rather focus on a phenomenological theory applicable to biosensors with various architectures. The model in Eq. (1) describes the steady state levels of the regulator (TF) and the target protein (P), and implicitly assumes that mRNA transcripts are also at steady state because mRNA half-lives are typically much shorter than protein lifetimes (30).

Under the phenomenological model in Eq. (1), the overall response of the biosensor is the composite function $P = f_2(f_1(M))$. The resulting dose-response curve has all the mathematical properties of a sigmoidal curve, namely, it is monotonically increasing, it has a single inflection point, and it approaches a finite limit value for large values of M. These properties hold for each of the four biosensor architectures in Figure 1A (see Supplementary File S1).

From biophysical considerations, it is typically assumed that mutations to the promoter operator site affect the TF-operator affinity (21, 26). In our phenomenological approach, we further assume that changes to TF-operator affinity can be captured by perturbations to the K_2 parameter only. This simplification allows us to model each strain in our library with a different value of K_2. We numerically computed the (μ,θ) parameters from the dose-response curves $P = f_2(f_1(M))$ for varying values of K_2, and fitted the model parameters to the (b,μ,θ) triplets from our fluorescence data (see Methods). Despite its simplified nature, the results in Figure 1D suggests that our phenomenological model qualitatively reproduces the observed relation between dynamic range and threshold, thus providing a simple method to map the impact of mutations to the operator site onto the biosensor dose-response curve.

Phenomenological theory for biosensor tuning

To further elucidate the constraints that underpin biosensor design, we obtained formulae for the dose-response parameters in terms of the tunable parameters**.** For the repressed-repressor architecture, described by the model in Eq. (1), the dose-response parameters are

$$b = b_2 + \frac{a_2}{1 + \left(K_2(b_1 + a_1)\right)^{n_2}}, \tag{2}$$

$$a = a_2 \cdot \frac{\left((b_1 + a_1)^{n_2} - b_1^{n_2}\right) \cdot K_2^{n_2}}{\left(1 + \left(K_2(b_1 + a_1)\right)^{n_2}\right) \cdot (1 + (b_1 K_2)^{n_2})}, \tag{3}$$

$$\theta = \frac{1}{K_1} \cdot \sqrt[n_1]{\frac{a_1 K_2}{\sqrt[n_2]{A-1} - b_1 K_2} - 1}\,, \tag{4}$$

where A is a function a_1, b_1, K_2, and n_2, shown in Supplementary File S1. For brevity, we report the computation of the biosensor sensitivity in Supplementary File S1.

From Eqs. (2) and (3), we compute the biosensor dynamic range as

$$\mu = \frac{a}{b} = \mu_2 \cdot \frac{\left((b_1 + a_1)^{n_2} - b_1^{n_2}\right) K_2^{n_2}}{\left(1 + \left(K_2(b_1 + a_1)\right)^{n_2} + \mu_2\right) \cdot \left(1 + (b_1 K_2)^{n_2}\right)}, \tag{5}$$

with $\mu_2 = a_2/b_2$ being the dynamic range of promoter expression. The formulae for the dose-response parameters of the other biosensor architectures (Figure 1A) can be found in the Supplementary File S1. The results in Eqs. (2)-(5) reveal that the dose-response parameters are coupled to one another through the TF-operator affinity (K_2). Changes to the operator sequence cause simultaneous changes to the basal output (b), dynamic range (μ) and response threshold (θ), in accordance with the dependency observed in our data in Figure 1C.

As shown in Figures 2A for a repressed-repressor architecture, for low TF-operator affinities (K_2) the biosensor produces an almost constitutive, metabolite-independent output, and thus displays low dynamic ranges. For increases in the K_2 parameter, the model predicts a decrease in basal biosensor output (b), with a relatively minor impact on the maximal output. This causes an increase in dynamic range and biosensor threshold, in agreement with what we observed in our lac promoter library (Figure 1D).

For high TF-operator affinities, however, our model predicts that the constraint between dynamic range and threshold depends strongly on the basal TF activity, modeled by the b_1 parameter in Eq. (1). In the case of the repressed-repressor architecture, the basal TF activity corresponds to the concentration of TF available for repression at maximum induction. When the b_1 parameter is nil, we found a monotonic relationship between biosensor dynamic range and threshold, but an increased b_1 parameter produces a non-monotonic dependency between them (Figure 2B). This constraint appears in all biosensor architectures (see Supplementary Figure SF1). In the case of the repressed-repressor architecture, this seemingly counterintuitive phenomenon arises because TFs with large basal activity (high b_1) will have some repressors available to bind to the operator site, even at full induction. Thus, at full induction, an increased TF-operator affinity causes a stronger binding by the available repressors, decreasing protein expression and lowering biosensor dynamic range (Figure 2B). In contrast, for TFs with negligible basal activity (low b_1) we do not observe such a drop in dynamic range (Figure 2A), because at full induction there are so few repressors available that protein expression is insensitive to the TF-operator affinity.

A consequence of the constraint in Figure 2B is that changes to the TF-operator affinity can tune the biosensor threshold within a limited range only. In the case of the repressed-repressor architecture, the theoretical limits for the biosensor threshold are

$$\theta_{\min} = \frac{1}{K_1} \cdot \left(\frac{\mu_1}{2^{-\frac{1}{n_2}} \cdot \left(1 + (1 + \mu_1)^{n_2}\right)^{\frac{1}{n_2}} - 1} \right)^{\frac{1}{n_1}}, \tag{6}$$

$$\theta_{\max} = \frac{1}{K_1} \cdot \left(\frac{\mu_1}{2^{\frac{1}{n_2}} \cdot \left(\frac{(1+\mu_1)^{n_2}}{1+(1+\mu_1)^{n_2}} \right)^{\frac{1}{n_2}} - 1} \right)^{\frac{1}{n_1}}, \quad (7)$$

where $\mu_1 = a_1/b_1$ is the dynamic range of TF activity. The limit thresholds for the other architectures can be found in Supplementary File S1. From the formula in Eq. (5) we also computed the maximal dynamic range that is achievable with changes to the TF-operator affinity:

$$\mu_{\max} = \mu_2 \cdot \frac{((1+\mu_1)^{n_2} - 1)}{\left((1+\mu_1)^{\frac{n_2}{2}} + (1+\mu_2)^{\frac{1}{2}} \right)^2}, \quad (8)$$

As shown in Supplementary File S1, the formula for $\mu_{\max}$ applies to all four biosensor architectures in Figure 1A. Since Eq. (8) scales with both μ_1 and μ_2, it suggests that the maximal dynamic range can be controlled by tuning the TF expression level (through parameter a_1) or by adjusting the promoter strength (through parameter a_2). Detailed examination of the formula for $\mu_{\max}$, however, reveals that it has a more pronounced dependency on μ_2, which is advantageous because according to Eqs. (2)-(4), parameter μ_1 also affects all the other dose-response parameters simultaneously.

Orthogonal control of dynamic range and threshold

The results in Eqs. (4) and (5) reveal two tunable parameters, promoter dynamic range (μ_2) and metabolite-TF affinity (K_1), that affect the biosensor dynamic range and threshold separately, whilst all remaining tunable parameters cause simultaneous changes in both. This means that μ_2 and K_1 can be used for orthogonal control of dynamic range and threshold. In particular, the phenomenological model predicts that μ_2 causes a vertical scaling in the (μ,θ)-curve, while K_1 scales it horizontally, as illustrated in Figure 2C. As shown in Supplementary File S1, we found that this strategy for orthogonal control is valid in all other biosensor architectures in Figure 1A, thus suggesting a general principle for biosensor design.

To test the predicted orthogonal control in our lac system, we used two complementary strategies. First, we induced our strains in Figure 1C with methyl-1-thio-β-d-galactopyranoside (TMG), another gratuitous lac inducer with an affinity to LacI approximately 10 times lower than IPTG (31), which in our model corresponds to a reduced K_1 parameter. Second, we built six new lac promoters in *E. coli*. In addition to mutating the operator sites, the promoter strength was modified by replacing the -35 and -10 regions of the *lacUV5* promoter with those of the sequences from promoter P_{A1} of phage T7. The P_{A1} promoter has a higher binding affinity to RNA polymerase (32), and hence an increased promoter strength, which in our model corresponds to an increased value for a_2 and μ_2.

We measured the dose-response curves of both sets of strains with RFP fluorescence, shown in Figure 3A-B, and quantified the dose-response parameters in Figure 3C. The results show a good qualitative agreement with our predictions. Strains with increased promoter strength display a larger dynamic range (Figure 3C, yellow), while a reduced metabolite-TF affinity caused an increase in response threshold (Figure 3C, blue), both with respect to our original strains in Figure 1C. We re-fitted the mathematical model for both sets of strains and observed that the model produces good fits in both cases. For the TMG-induced strains (blue curve, Figure 3C), we used the parameters from the IPTG experiments (Figure 1C) and re-fitted K_1 and b_1. Although we only expected a change in K_1, we were unable to produce good fits without also re-fitting parameter b_1. This is possibly because a lower affinity decreases the probability of TMG binding, and so at full induction there are fewer repressors bound to TMG, as compared to those bound to IPTG, resulting in a higher b_1. For the strains with a promoter sequence perturbed at the -35 and -10 regions (yellow curve, Figure 3C), we used the parameters from the IPTG strains (Figure 1C) and re-fitted a_2, b_2 and n_2. We expected the P_{A1} promoter sequence to affect parameter a_2 only, but we needed to re-fit b_2 and n_2 as well. This

suggests biophysical couplings between tunable parameters that are not included in our model. Nevertheless, the results suggest that biosensor dynamic range increases with the $\mu_2 = a_2/b_2$ parameter, with negligible impact on the biosensor threshold, in agreement with our theoretical prediction.

To verify whether the changes in dynamic range and threshold were indeed orthogonal for changes in K_1 and μ_2, we focused on three sets of strains, A_1 and A_2, B_1 and B_2, and C_1 and C_2, shown in Figure 3C. Strains within each set share the same operator sequence, but differ in the sequence of their -35 and -10 promoter regions. This enables us to survey the impact on the response parameters for changes in the two tunable parameters for each set of strains. A comparison of their response parameters, shown in Figure 3D, validate the predicted orthogonal control: a decrease in metabolite-TF affinity caused a large change in dose-response threshold and relatively small change in dynamic range, while a change in promoter strength caused a negligible change in threshold but a large shift in dynamic ranges.

Discussion

In this work we identified quantitative principles for the design of metabolite biosensors. Previous research on biosensors has focused primarily on expanding the repertoire of detectable metabolites (14, 33, 34). Most applications, however, require some degree of tunability on the biosensor dose-response curve, an aspect that remains poorly understood but is fundamental for their broad applicability. Given the substantial effort required to build new biosensors, a quantitative understanding of how tunable parameters shape biosensor function can help narrow down the design space, single out useful architectures, and determine the best experimental strategies to tune them.

Using the lac promoter in *E. coli* as a model system, we showed that mutations in the operator sequence simultaneously affect the basal output, dynamic range, and threshold of the dose-response curve. Such coupling between dose-response parameters makes it challenging to control biosensor function without a quantitative guideline. We quantified the parameter dependencies with a simple phenomenological model in which common tunable parameters such as TF-operator affinity, promoter strength and TF expression level can be readily incorporated, thus providing a widely applicable theory for biosensor design. Our theory revealed that upon changes in operator affinity, metabolite-responsive TFs are subject to design constraints between dynamic range and response threshold. These constraints become more severe for 'leaky' TFs that have a large basal activity, because they display a maximal achievable dynamic range that cannot be overcome by changes to the operator site.

We also found that biosensor dynamic range and threshold can be controlled orthogonally with the promoter dynamic range and the TF-metabolite binding affinity. Our models predict that this design principle holds for all considered biosensor architectures. Numerous promoter engineering techniques can be used to rapidly change promoter properties (20, 35, 36). Although changes to the TF-metabolite binding are significantly more challenging, recent progress in protein engineering have showcased the construction of metabolite-responsive TFs with perturbed affinities to their cognate ligands (19, 37), and even modified to bind to new molecules (14, 15). Our results suggest that promoter libraries with combinatorial designs for operator site and promoter strength cover a large portion of the design space for the biosensor dynamic range, whilst TF engineering can help to control the sensing threshold of leaky TFs.

Tunability of biosensors is essential for precision engineering of metabolism. In dynamic pathway engineering, biosensors control the expression of catalytic enzymes and are core components of feedback loops that re-route metabolic flux in response to pathway intermediates. For example, tuning the response curves of acyl-CoA and malonyl-CoA biosensors helped to increase production of fatty acid and fatty acid-derived fuels in *E. coli* (1, 2). With adequate tuning of the biosensor dose-response curve, feedback-regulated pathways can adapt their enzyme levels to the metabolic status of the host, prevent the accumulation of toxic intermediates, and control pathway variability (3, 4, 16, 38). The

design constraints we have reported here thus highlight the need for comprehensive characterization of biosensor libraries. The common approach of tuning biosensors based on dynamic range alone neglects potential knock-on effects on the sensing threshold, which may render a biosensor unresponsive to the physiological concentrations of a target metabolite.

Our theory has exposed design constraints applicable to biosensors with any of the four architectures in Figure 1A. Biosensors with various architectures have been already developed for a number of applications (10, 11). Our results provide a quantitative framework for controlling dynamic range and threshold in these biosensors, beyond the repressed-repressor architecture we have studied here. For example, the activated-activator architecture can be found in biosensors based on the TyrR regulator (5), while the repressed-activator and activated-repressor architectures can be found in biosensors based on SoxR and BetI, respectively (19, 39); see Table SF2 in the Supplementary File S1 for more examples. Furthermore, here we focused on design constraints under a variable operator affinity, as this is one of the most common tunable parameters. Our theory can be extended to uncover constraints for other tunable parameters accessible in specific applications, such as variable promoter strengths (a_2 parameter) or promoter sensitivity (n_2 parameter), which can be implemented with promoter libraries with variable RNA polymerase binding sites (36) or operator copy number (2). We also expect the use of other tunable parameters, such as the TF expression level, to produce more drastic changes in dose-response curves than those we observed here, for example by affecting the basal and maximal output simultaneously.

In this work we have deliberately used phenomenological models because they provide a versatile tool to explore the parameter space for various biosensor architectures. The drawback of this simplification is that it overlooks the specific mechanisms for metabolite-TF binding and TF regulation (25). Our models also inherently assume that the tunable parameters are independent from one another, yet in reality they are coupled through the biophysical interactions between the TF, promoter and other transcriptional components such as RNA polymerases and σ-factors, which may produce further design constraints (21, 22). Although our data showed some effects that cannot be fully explained by our models, overall we found that our phenomenological theory provides a good first approximation to link design parameters with biosensor dose-response curves. Our approach revealed constraints in dose-response curves for common tunable parameters, providing a quantitative basis to identify useful biosensor architectures and to determine suitable experimental strategies for biosensor tuning.

Unlike most other engineering disciplines, synthetic biology suffers from a limited availability of sensing devices. Our work has uncovered fundamental design principles for metabolite biosensors, which in light of the tremendous progress in DNA, RNA and protein engineering, are essential to bring precision metabolic engineering closer to reality.

METHODS

Mathematical modeling and curve fitting

The phenomenological models were built through the composite function $P = f_2(f_1(\mathrm{M}))$, where f_1 and f_2 are increasing or decreasing Hill functions. The function $P(M)$ is monotonic in M, has a single inflection point, and reaches its extremal values at $M = 0$ and $M \to \infty$, thus resembling a sigmoid function. We obtained the biosensor parameters a and b from the definitions

$$a = \max f_2\big(f_1(M)\big) - \min f_2\big(f_1(M)\big),$$
$$b = \min f_2\big(f_1(M)\big),$$

for $M \geq 0$, from where the dynamic range is $\mu = a/b$. We computed the response threshold θ as the solution of the equation

$$f_2\big(f_1(\theta)\big) = b + \frac{a}{2},$$

which represents the metabolite concentration for 50% output, relative to the basal. The computation of the dose-response sensitivity is explained in Supplementary File 1. The upper and lower bounds on μ and θ were computed by differentiation with respect to TF-operator affinity K_2 (details in

Supplementary File S1). Equations (2)-(7) are valid for the repressed-repressor architecture, while Eq. (8) for the maximal dynamic range is valid for all architectures. Details of the derivation and formulae of dose-response parameters in all architectures are given in Supplementary File S1.

For the parameter fitting in Figures 1D and 3C, we obtained the dose-response parameters from the promoter characterization data, $\mu_{i,E}$, $\theta_{i,E}$ and $b_{i,E}$, of the i^{th} strain for each of the three sets of experiments. The dynamic range ($\mu_{i,E}$) and basal expression level ($b_{i,E}$) were calculated from the data at zero and full induction, and the threshold ($\theta_{i,E}$) from fits of a Hill function to the data. The model predictions (μ_E, b_E, θ_E) were generated from equations (2)-(5) evaluated over a fixed range of K_2 from K_2=3×10^{-5} to K_2=10^3, with the other seven parameters $p = (a_1, b_1, K_1, n_1, a_2, b_2, n_2)$ fitted to the data triplets ($\mu_{i,E}$, $\theta_{i,E}$, $b_{i,E}$) via nonlinear least-squares. We solved the optimization problem

$$\min_p \sum_{i=1}^{\#\,\text{Strains}} \left(\frac{\mu_{i,E} - \mu_{i,M}(K_{2,i}, p)}{\hat{\mu}_E}\right)^2 + \left(\frac{\theta_{i,E} - \theta_{i,M}(K_{2,i}, p)}{\hat{\theta}_E}\right)^2 + \left(\frac{\log_{10} b_{i,E} - \log_{10} b_{i,M}(K_{2,i}, p)}{\log_{10} \hat{b}_E}\right)^2,$$

where $\mu_{i,M}$, $\theta_{i,M}$ and $b_{i,M}$ are computed from equations (2)-(5) and $K_{2,i}$ corresponding to the value of K_2 where the model prediction is closest to the i^{th} data point. Each term of the objective is normalized by the maximum measured value, denoted $\hat{\mu}_E$, $\hat{\theta}_E$ or $\hat{b}_E$. In Figure 1D we fitted all model parameters. The green line is a model fit with parameters reported in Table SF1 in Supplementary File S1. In Figure 3C (blue) we used the fitted parameters from Figure 1D (green) and re-fitted K_1 and b_1. In Figure 3C (yellow), we used the parameters from Figure 1D (green) and refitted a_2, b_2 and n_2. Further details on the parameter fitting can be found in Supplementary File 1. The parameter fitting was done through 500 runs of the fmincon solver using the multistart routine from the MATLAB Global Optimization toolbox.

Construction and characterization of promoters

The lac promoter libraries were constructed by introducing mutations to the lac operator site in a Biobrick plasmid pBbB5k-RFP (40). The P_{A1} promoter library (increased μ_2) was cloned by switching the -35 and -10 regions of the LacUV5 promoter to those of P_{A1} promoter from phage T7 (sequence shown in Figure 3B), yielding plasmid pBbB5pgk-RFP. To vary the K_2 parameter, two lac promoter libraries were created with operator sequences AATTGTGANNNGATAACAATT and AANNNTGAGCGGATAACAAT (Figure 1C, 3A & 3B), generating a strain library with the size of 128 sequences. The lac promoter libraries were constructed using a one-step Golden-Gate DNA assembly method and were then transformed into MG1655 cells. The promoter libraries were pre-screened from a random selection of colonies from the whole library, and the ones with relatively high and distinct dynamic ranges were selected for further characterization.

Cell growth and fluorescence were recorded on an Infinite F200PRO (Tecan) plate reader. Strains were first cultivated overnight in Luria-Bertani (LB) medium supplemented with 50 mg/L kanamycin. The overnight LB cultures of the lac promoter strains were inoculated 2% v/v into M9 medium supplemented with 1% glycerol, 50 mg/L kanamycine, and amino acids, composed as for the EZ-rich medium (41) for adaptation. The overnight culture was inoculated 2% v/v into the same medium and grew to an OD_{600} of 0.6. Cell cultures were then diluted by 30-fold in the same medium and induced with varying IPTG (0.1, 1, 4, 10, 40, 100, 400, and 1000 μM) and TMG (1, 100, 400, 1000, 2000, 4000, 10000, and 40000 μM) concentrations.

Cell density (OD_{600}) and red fluorescence (excitation: 535 ± 9 nm; emission: 620 ± 20 nm) were recorded every 1000 s until the cell culture reached the stationary phase. Fluorescence from a wild-type *E. coli* MG1655 cell culture was used as the background, and was subtracted from all fluorescence measurements. The background-corrected fluorescence was later normalized by cell density as measured at OD_{600}. Cells were maintained in the exponential growth phase for 5-6 cell cycles until the normalized fluorescence reached to the steady state, and the steady state fluorescence were used to generate the dose-response curves. We extracted the biosensor parameters (b, μ, θ) from Hill functions fitted to the measured dose-response curves. Standard errors

of the dose-response parameters were calculated from the fitted parameters of the response curves for biological replicates, for each strain.

SUPPLEMENTARY INFORMATION

- Supplementary Information S1: Mathematical models and analyses in terms of tunable parameters.
- Supplementary Information S2: Promoter characterization data MS Excel format.

AUTHOR CONTRIBUTIONS

A.M. and D.O developed and analyzed the mathematical models. D.L. and F.Z. constructed and characterized all strains. D.O and F.Z. conceived the project and designed the research. All authors analyzed data and model predictions.

ACKNOWLEDGEMENTS

This work was funded by the Human Frontier Science Program through a Young Investigator Grant awarded to D.O and F.Z. (Grant no. RGY0076-2015) and the US National Science Foundation (MCB1453147) to F.Z.

REFERENCES

1. Zhang F, Carothers JM, Keasling JD (2012) Design of a dynamic sensor-regulator system for production of chemicals and fuels derived from fatty acids. *Nat Biotechnol* 30(4):354–9.
2. Xu P, Li L, Zhang F, Stephanopoulos G, Koffas M (2014) Improving fatty acids production by engineering dynamic pathway regulation and metabolic control. *Proc Natl Acad Sci* 111(31):11299–11304.
3. Oyarzún DA, Stan G-B V (2013) Synthetic gene circuits for metabolic control: design trade-offs and constraints. *J R Soc Interface* 10(78). doi:10.1098/rsif.2012.0671.
4. Dunlop MJ, Keasling JD, Mukhopadhyay A (2010) A model for improving microbial biofuel production using a synthetic feedback loop. *Syst Synth Biol* 4(2):95–104.
5. Xiao Y, Bowen CH, Liu D, Zhang F (2016) Exploiting nongenetic cell-to-cell variation for enhanced biosynthesis. *Nat Chem Biol* 12(5):339–344.
6. Rogers JK, et al. (2015) Synthetic biosensors for precise gene control and real-time monitoring of metabolites. *Nucleic Acids Res* 43(15):7648–7660.
7. Oyarzún DA, Chaves M (2015) Design of a bistable switch to control cellular uptake. *J R Soc Interface* 12(20150618). doi:doi: 10.1098/rsif.2015.0618.
8. Beisel CL, Smolke CD (2009) Design principles for riboswitch function. *PLoS Comput Biol* 5(4):e1000363.
9. Berens C, Suess B (2015) Riboswitch engineering - making the all-important second and third steps. *Curr Opin Biotechnol* 31:10–15.
10. Liu D, Evans T, Zhang F (2015) Applications and advances of metabolite biosensors for metabolic engineering. *Metab Eng* 31:35–43.
11. Mahr R, Frunzke J (2016) Transcription factor-based biosensors in biotechnology: current state and future prospects. *Appl Microbiol Biotechnol* 100(1):79–90.
12. Chubukov V, Gerosa L, Kochanowski K, Sauer U (2014) Coordination of microbial metabolism. *Nat Rev Microbiol* 12(5):327–40.
13. Skjoedt ML, et al. (2016) Engineering prokaryotic transcriptional activators as metabolite biosensors in yeast. *Nat Chem Biol* 12(11):951–958.
14. Taylor ND, et al. (2016) Engineering an allosteric transcription factor to respond to new ligands. *Nat Methods* 13(2):177–183.
15. Tang S-Y, Cirino PC (2011) Design and application of a mevalonate-responsive regulatory protein. *Angew Chem Int Ed Engl* 50(5):1084–1086.
16. Liu D, Xiao Y, Evans BS, Zhang F (2015) Negative feedback regulation of fatty acid production based on a malonyl-CoA sensor-actuator. *ACS Synth Biol* 4(2):132–140.
17. Xu P, et al. (2014) Design and Kinetic Analysis of a Hybrid Promoter–Regulator System for Malonyl-CoA Sensing in Escherichia coli. *ACS Chem Biol* 9(2):451–458.
18. Chou HH, Keasling JD (2013) Programming adaptive control to evolve increased metabolite production. *Nat Commun* 4:2595.
19. Saeki K, Tominaga M, Kawai-Noma S, Saito K, Umeno D (2016) The rapid diversification of BetI-based transcriptional switches for the control of biosynthetic pathways and genetic circuits. *ACS Synth Biol*. doi:10.1021/acssynbio.5b00230.
20. Blazeck J, Alper HS (2013) Promoter engineering: recent advances in controlling transcription at the most fundamental level. *Biotechnol J* 8(1):46–58.
21. von Hippel PH, Berg OG (1986) On the specificity of DNA-protein interactions. *Proc Natl Acad Sci U S A* 83(6):1608–12.
22. Bintu L, et al. (2005) Transcriptional regulation by the numbers: Models. *Curr Opin Genet Dev* 15(2):116–124.
23. Martins BMC, Swain PS (2011) Trade-Offs and Constraints in Allosteric Sensing. 7(11):1–13.
24. Ang J, Harris E, Hussey BJ, Kil R, McMillen DR (2013) Tuning response curves for synthetic biology. *ACS Synth Biol* 2(10):547–67.

25. de Paepe B, Peters G, Coussement P, Maertens J, de Mey M (2016) Tailor-made transcriptional biosensors for optimizing microbial cell factories. *J Ind Microbiol Biotechnol*:1–23.
26. Garcia HG, et al. (2012) Operator sequence alters gene expression independently of transcription factor occupancy in bacteria. *Cell Rep* 2(1):150–161.
27. Yagil G, Yagil E (1971) On the Relation between Effector Concentration and the Rate of Induced Enzyme Synthesis. *Biophys J* 11(1):11–27.
28. Buchler NE, Cross FR (2009) Protein sequestration generates a flexible ultrasensitive response in a genetic network. *Mol Syst Biol* 5:272.
29. Bintu L, et al. (2005) Transcriptional regulation by the numbers: Applications. *Curr Opin Genet Dev* 15(2):125–135.
30. Bremer H, Dennis P (1996) Modulation of chemical composition and other parameters of the cell by growth rate. In Escherichia coli and Salmonella typhimurium. *Neidhardt, F (ed) Washington, DC Am Soc Microbiol Press* (122):1553.
31. Marbach A, Bettenbrock K (2012) lac operon induction in Escherichia coli: Systematic comparison of IPTG and TMG induction and influence of the transacetylase LacA. *J Biotechnol* 157(1):82–88.
32. Lanzer M, Bujard H (1988) Promoters largely determine the efficiency of repressor action. *Proc Natl Acad Sci U S A* 85(23):8973–7.
33. Younger AKD, Dalvie NC, Rottinghaus AG, Leonard JN (2017) Engineering Modular Biosensors to Confer Metabolite-Responsive Regulation of Transcription. *ACS Synth Biol* 6(2):311–325.
34. Nadler DC, Morgan S-A, Flamholz A, Kortright KE, Savage DF (2016) Rapid construction of metabolite biosensors using domain-insertion profiling. *Nat Commun* 7:12266.
35. De Mey M, et al. (2010) Promoter knock-in: a novel rational method for the fine tuning of genes. *BMC Biotechnol* 10:26.
36. Brewster RC, Jones DL, Phillips R (2012) Tuning promoter strength through RNA polymerase binding site design in Escherichia coli. *PLoS Comput Biol* 8(12):e1002811.
37. Richards DH, Meyer S, Wilson CJ (2017) Fourteen Ways to Reroute Cooperative Communication in the Lactose Repressor: Engineering Regulatory Proteins with Alternate Repressive Functions. *ACS Synth Biol* 6(1):6–12.
38. Oyarzún DA, Lugagne J-B, Stan G-B (2014) Noise propagation in synthetic gene circuits for metabolic control. *ACS Synth Biol*. doi:10.1021/sb400126a.
39. Siedler S, et al. (2014) SoxR as a single-cell biosensor for NADPH-consuming enzymes in Escherichia coli. *ACS Synth Biol* 3(1):41–47.
40. Mason G, et al. (2002) BglBrick vectors and datasheets: A synthetic biology platform for gene expression. *BMC Biotechnol* 2(1):20.
41. Neidhardt FC, Bloch PL, Smith DF (1974) Culture Medium for Enterobacteria. *J Bacteriol* 119(3):736–747.

FIGURES

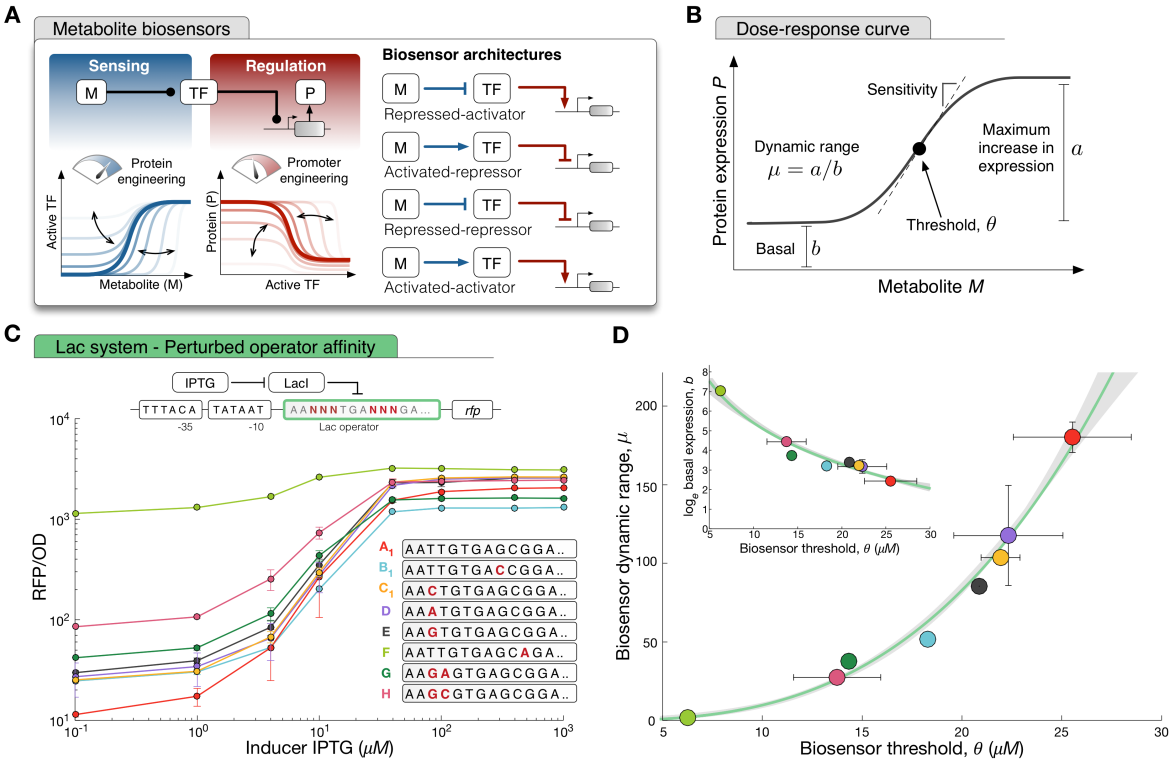

Figure 1. Design constraints in dose-response curves of metabolite biosensors.
(A) General architecture of biosensors based on metabolite-responsive transcription factors (TF). The metabolite (M) interacts with a TF that controls expression of a target protein (P). The sensing and regulation modules can be tuned with protein and promoter engineering. **(B)** Parameters that characterize a biosensor dose-response curve: basal output (b); response threshold (θ), defined as the amount of metabolite required for 50% output expression relative to the baseline; dynamic range (μ), defined as the maximal increase in expression relative to the basal output; response sensitivity, defined as the slope of the dose-response curve at the threshold. **(C)** Dose-response curves of LacI-based biosensors with variable operator sites, in response to IPTG induction. Error bars represent standard error from biological replicates; some error bars are too small to be observed. **(D)** Dose-response parameters of the strains in panel C, and fit of the phenomenological model in Eq. (1), green line. Error bars are the standard error of measured dose-response parameters across biological replicates; some error bars are too small to be observed. The gray band contains model predictions for 500 runs of the parameter estimation algorithm; the solid green line is the fit for a specific parameter set. Further details on the model fitting can be found in Supplementary File 1.

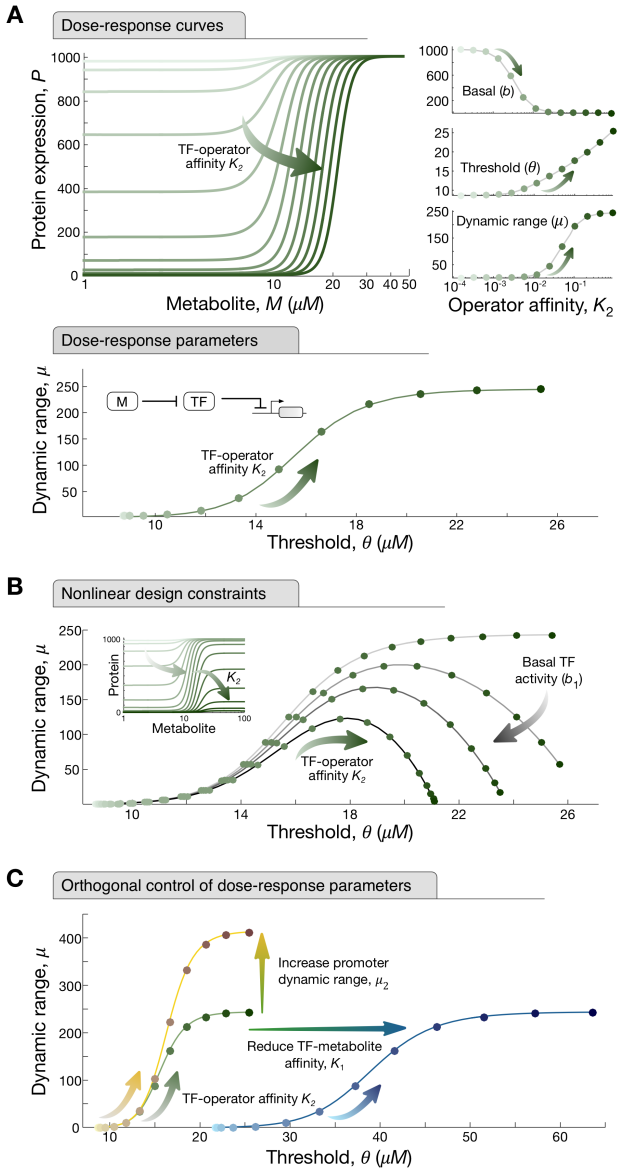

Figure 2. Control of biosensor dose-response curves with tunable parameters.
(A) Dose-response curves predicted from the model for biosensors with variable operator affinities. Our phenomenological theory predicts that tighter TF-operator binding leads to a lower basal output and a broader dynamic range, accompanied by an increased biosensor threshold. The bottom plot shows how this coupling between dynamic range (μ) and threshold (θ) constrains biosensor function, in agreement with the behavior observed from our data in Figure 1C-D. Parameter values are: a_1 = 300, a_2 = 1000, b_1 = 0.01, b_2 = 4.1, n_1 = 6, n_2 = 2, K_1 = 0.1, and K_2 values span the range K_2 = 0.0005 to K_2 = 0.9; all concentrations in μM. **(B)** Increased basal TF activity (b_1) leads to highly nonlinear constraints between dynamic range and threshold. Plots show increasing values of the b_1 parameter, from b_1 = 0.01 up to b_1 = 8. The inset shows the dose-response curves for increasing operator affinities (K_2), at a relatively high basal TF activity (b_1 = 8). **(C)** Two tunable parameters, the promoter dynamic range (μ_2) and TF-metabolite affinity (K_1), provide orthogonal control and scale the dynamic range and threshold. Parameter values are the same as in panel A, except a_2 = 1700 (yellow curve) and K_1 = 0.04 (blue curve). In all panels, plots shown are for the repressed-repressor architecture, but the conclusions apply to all biosensor architectures in Figure 1A, see Supplementary File S1.

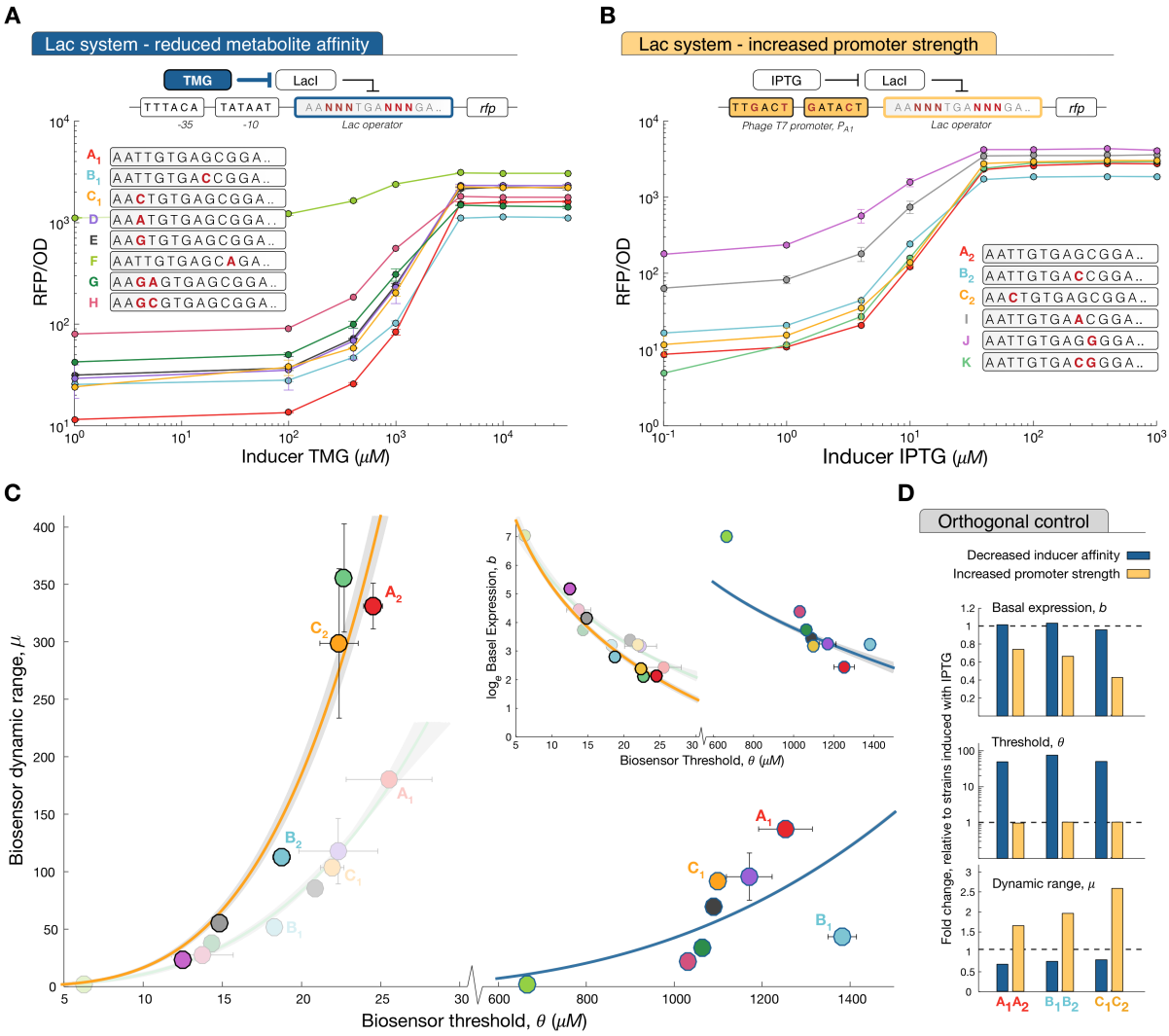

Figure 3: Orthogonal control of biosensor dynamic range and threshold.
(A) Dose-response curves of the lac strains from Figure 1C induced with TMG, which has a 10-fold lower affinity to LacI than IPTG. **(B)** Dose-response curves of strains with variable operator sites and increased promoter strength. Error bars represent standard error from biological replicates; some error bars are too small to be observed. **(C)** Dose-response parameters and model fits of strains in panel A (blue curve), and panel B (yellow curve). For comparison, the parameters of the IPTG-induced strains (Figure 1D) are shown here in light gray. Error bars are the standard error of measured dose-response parameters across biological replicates; some error bars are too small to be observed. The gray bands contain model predictions for 500 runs of the parameter estimation algorithm. The solid lines (blue, yellow) are fits for specific parameter sets; the gray band of the blue curve is too small to be observed. Further details on the model fitting can be found Supplementary File 1. **(D)** Validation of the predicted orthogonal control of dynamic range and threshold. We focused on three sets of strains (A_i, B_i, C_i) that are comparable across the three experiments. Strains within each set share the same operator sequence, but differ in their -35, -10 promoter region sequence. Bar plots show the fold change in dose-response parameters for a decreased inducer affinity or increased promoter strength, with respect to strains in Figure 1D.

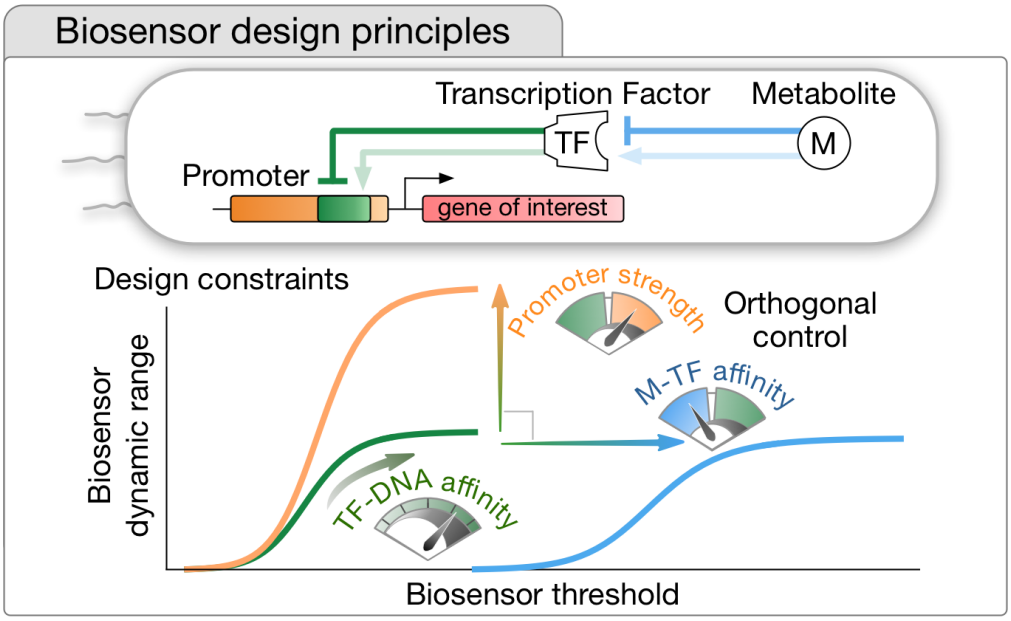

TOC Figure / Graphical abstract.